IEEE Access
Multidisciplinary | Rapid Review | Open Access Journal

Received 16 February 2024, accepted 1 March 2024, date of publication 5 March 2024, date of current version 13 March 2024.

Digital Object Identifier 10.1109/ACCESS.2024.3374198

RESEARCH ARTICLE

A Novel Fault Detection and Location Approach for DC Zonal Shipboard Microgrid Based on High-Frequency Impedance Estimation With IEC 61850 Communication Protocol

ASMAA M. ABOELEZZ[1], MAGDI M. EL-SAADAWI[1], ABDELFATTAH A. ELADL[1], VLADIMÍR BUREŠ[2], AND BISHOY E. SEDHOM[1], (Member, IEEE)

[1]Electrical Engineering Department, Faculty of Engineering, Mansoura University, Mansoura 35516, Egypt
[2]Faculty of Informatics and Management, University of Hradec Králové, 50003 Hradec Králové, Czech Republic

Corresponding authors: Vladimír Bureš (vladimir.bures@uhk.cz) and Bishoy E. Sedhom (eng_bishoy90@mans.edu.eg)

This work was supported in part by the Faculty of Informatics and Management, University of Hradec Králové (UHK), through the Specific Research Project "Addressing Modern Research Topics With Increased Student Involment."

ABSTRACT This paper introduces an innovative adaptive scheme for detecting and locating faults in DC-zonal shipboard microgrids (SBMGs). This scheme relies on the estimation of high-frequency impedance. The proposed scheme is implemented in an intelligent electronic device (IED) in which the Fast Fourier Transform is applied to obtain the high-frequency components of the current and voltage at each node. Then, these components are exchanged between the two IEDs that protect the same line by using IEC 61850 GOOSE-based communication system. The estimated high-frequency impedance of the line is calculated and compared to the prescribed settings to detect and locate the fault. After fault detection and localization, communication signals are exchanged between the two IEDs positioned at each end of the line. This exchange precedes the transmission of tripping signals to the relevant circuit breakers for the accurate isolation of the faulty line. The proposed protection scheme is tested through MATLAB/Simulink®environment. The scheme can detect and locate the fault under different uncertainty conditions, such as fault impedances, various system configurations, changes in system loads and generations, multi-faults' existence, contingency conditions, and the presence of noise on the communication signals. The results proved its efficient performance and superiority. The scheme can detect and locate the faults quickly and accurately within 0.125 ms.

INDEX TERMS Novel protection scheme, IEC 61850, fault detection, fault localization, DC zonal shipboard microgrid, high-frequency impedance estimation.

NOMENCLATURE

ABBREVIATIONS

ACSI	American Customer Satisfaction Indexes.
ATG	Auxiliary turbine generator.
CTWCS	Clearing time with the communication signals.
CTWOCS	Clearing time without the communication signals.
ESS	Energy Storage System.
FFT	Fast Fourier transform.
GOOSE	Generic Object-Oriented Substation Event.
HFIE	High frequency impedance estimation.
HMIs	Human-machine interfaces.
IED	Intelligent electronic device.
KVL	Kirchhoff's voltage law.
MMS	Multimedia Messaging Service.
MTG	Main turbine generator.
OSI	Open Systems Interconnection.
PV	Photovoltaic.

The associate editor coordinating the review of this manuscript and approving it for publication was Qiang Li.

SBMGs	Shipboard microgrids.
SCN	Substation communication network.
SNR	Signal-to-noise ratio.
SPSs	Shipboard power systems.
SVs	Sampled values.
TCP/IP	Transmission Control Protocol/Internet Protocol.
WAN	Wide area network.

VARIABLES

ΔU_{MN}	The voltage difference between node M & node N.
I_F	Fault current.
I_M	the high-frequency voltage component at node M.
I_N	the high-frequency voltage component at node N.
L_M	the equivalent inductance of the line from node M to the fault location.
L_N	the equivalent inductance of the line from node N to the fault location.
L_U	unit inductance for the line.
L_l	the overall equivalent inductance of the line.
R_M	the equivalent resistance of the line from node M to the fault location.
R_N	the equivalent resistance of the line from node N to the fault location.
R_U	unit resistance for the line.
R_f	the fault resistance.
R_l	the overall equivalent resistance of the line.
S_M	communication signal of IED at node M.
S_N	communication signal of IED at node N.
U_M	the high-frequency component of voltage at node M.
U_N	the high-frequency component of voltage at node N.
$w\,(n)$	the signal that may be voltage or current.
Z_l	the line impedance.
t_{CB}	Circuit breaker time.
t_{clear}	Fault clearing time.
t_{comm}	Communication time.
$t_{detection}$	Fault detection time.
N	length of the Blackman window.
Z	the impedance between node M and the fault point.
d	the fault distance.
j	number of samples.
k	frequency index.
n	time index.
Δt	sample period.

I. INTRODUCTION

To meet the challenges of the modern maritime industry, shipboard power systems (SPSs) are evolving. These advancements address the issues related to efficient energy utilization and strive to minimize environmental impacts. SPSs have evolved for almost two decades since the beginning of the industrial revolution, especially to minimize pollutants and greenhouse gas emissions, which are concerns worldwide [1], [2]. In this new era, ships must be efficient and have lower fuel consumption. The SPSs are designed to provide power to all parts of the ship, including service loads and electric propulsion drives. SPS can be defined as a SBMG that operates in stand-alone mode during ship sailing [3], [4], [5]. DC distribution is a hot topic in the SPS community, in which All energy sources are linked to either an AC/DC converter or a DC/DC converter, and these converters are subsequently connected to a DC bus that transmits power to the load, as illustrated in Fig. 1. Compared to AC-SPSs, DC-SPSs have many benefits including [6], [7]: 1) there is no need for single-phase synchronization, 2) reducing the vessel weight and size due to eliminating large transformers, 3) fuel consumption reduction due to the use of a variable speed prime-mover, 4) managing power flow after faults, 5) simplifying the power sources' connection and disconnection, and 6) managing the disturbances and faults efficiently by utilizing the controlled power electronics devices.

The growing need for modern zonal marine power systems has arisen from the widespread usage of power electronics, the advancement of integrated electrical propulsion, and the rise in high-energy electrical demands. Zonal architectures can potentially provide a superior capability for fault ride-through and higher degree of power quality. The protection schemes of the short-circuit faults for the DC zonal distribution in SPSs have many challenges, such as the coordination of the protection devices and the power electronics to provide a robust protection system, the fault current changes when operating in the islanded mode, difficulty in designing a grounding system, severe transient discharge, and lack of current zero-crossing point which leads to an arc flash in the circuit breaker. The challenges also include the increase in the physical burden of the protection system (such as DC breakers), dynamic characteristics of renewable resources, bidirectional power flow, and the presence of pulsed loads with its smaller scale that are resulting in short circuit impedance differences in various locations [3], [8], [9], [10], [11], [12]. The existence of pulsed loads presents a challenge in distinguishing between normal and fault currents, as these loads have a large peak power and high-power change rate. Moreover, the ships are exposed to various uncertainties, including; The fluctuation in photovoltaic (PV) output power due to ship movement, even with constant solar radiation [13], and uncertainties related to weather conditions like wave parameters (height and length) and wind characteristics (speed and direction) introduce variability in navigation resistance during the voyage. Thus, the ship's propulsion loads differ according to the various navigation uncertainties [14], [15], [16], [17]. Such uncertainties affect the performance of the traditional protection schemes used in SPS. Furthermore, keeping the crew safe is essential; hence, a ship's electrical appliances should be monitored to detect excessive leakage

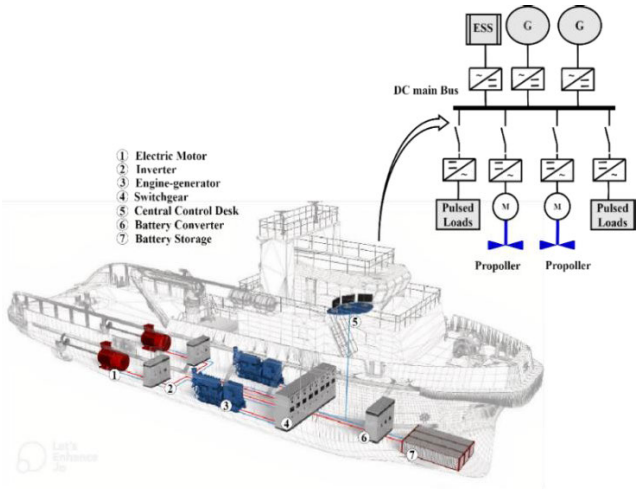

FIGURE 1. DC shipboard microgrid architecture.

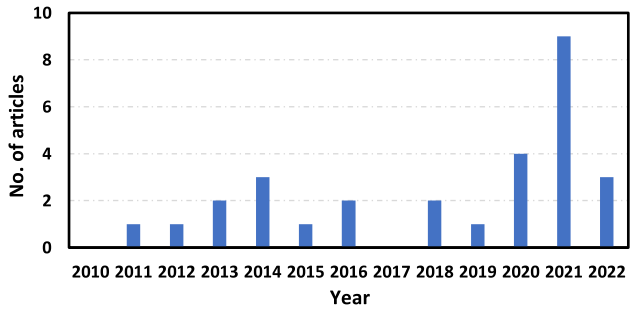

FIGURE 2. Research trend from 2010 to 2022.

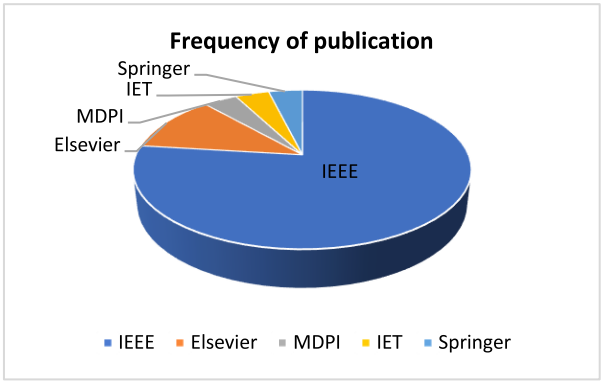

FIGURE 3. Published articles distribution based on different journals.

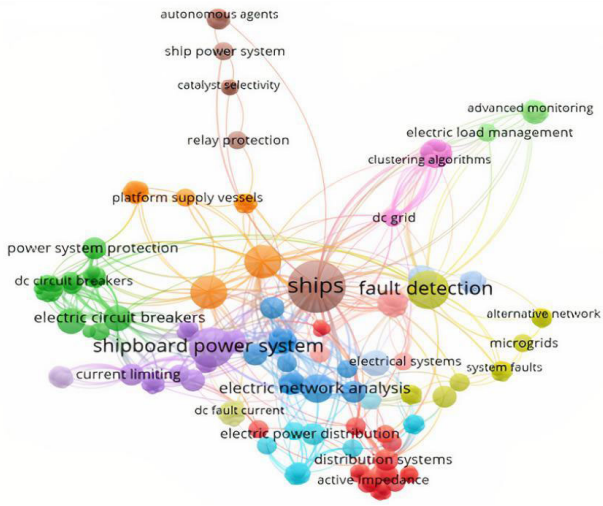

FIGURE 4. Co-occurrence analysis for protection articles concerning SBMGs.

currents flowing from the live parts to the ground [3], [18], [19], [20]. Besides, there are some common features of commercial and naval DC SPS, including 1) the low inductances of the short lines due to its limited space, 2) existance of multiple capacitors connected to the DC link, 3) the dynamic behavior of the loads, 4) the presence of distributed generators and their dynamic behavior, and 5) the probability of system instability as the generating capacity is comparable to the load demand [21]. These features also complicate the protection system of DC SPS. It is essential to identify, locate, and isolate faults within each zone to ensure the integrity of the healthy power system. Accordingly, the aforementioned challenges should be carefully treated to provide a reliable and safe protection system. Thus, it is essential to achieve a fast, simple, and adequate protection scheme to safeguard the reliability and security of zonal SBMG due to its complex structure. However, the main motivation behind the utilization of ring and zonal configurations in naval systems stems from the stringent demands for reliability and survivability.

To explore the importance of the protection system for SBMGs, a survey is performed on the Scopus database to find the related researches. A bibliometric analysis is done to find the recent trends in this field, and 29 articles are found from 2011 to 2022. The distribution of these articles for each year is shown in Fig. 2. It is noticed that the interest in this research trend has increased recently from 2020 until now. The distribution of the articles according to the journal publisher is shown in Fig. 3. Most of these articles (77%) were published by IEEE journals, followed by Elsevier (14%), followed by MDPI, IET, and Springer journals. Besides, a bibliometric analysis is performed for these articles using the VOS viewer program [22]. Co-occurrence analysis for protection articles concerning SBMGs is performed and illustrated in Fig. 4. It is concluded that the most crucial topic in this field is fault detection and location methods, especially for DC zonal SBMG.

The protection applied in DC SBMG for detecting and locating the fault could be divided into two categories that are: time domain measurement-based protections; and frequency domain measurement-based protections. Time domain measurement-based protections can be divided into two categories based on communication requirements. These categories are non-unit protection and unit protection systems. For non-unit protection, it uses locally measured information (without any communication) to identify the DC faults [23], such as overcurrent protection [24], [25].

Ref. [24] adopted overcurrent-based protection to meet the fast response requirements in fault detection and localization. However, the authors showed that this scheme could only localize the faults to the zones upstream/downstream of the converters. In contrast, Ref. [25] involved the voltage source converters to act similar to crowbars in series with an overcurrent relay for fault isolation from the generator's AC side in DC SPS. However, this scheme cannot be implemented for C.Bs on the DC side. The overcurrent protection scheme is limited because of its malfunction in the presence of pulsed loads and propulsion [3]. Besides, the artificial neural network-based method can grasp the fault data features to provide accurate decisions for protection. This method requires a massive system database for training and is incapable of online fault localization [26], [27]. On the other hand, artificial neural networks still have challenges like heavy computational burdens and complicated parameter selection [28]. However, the existence of high operational experience is important for applying a suitable threshold setting for the above protections.

As for unit protections, it requires communications that naturally have clear boundaries. The IEC 61850 communication protocol is the commonly used protocol in protection systems. It represents a globally recognized communication protocol employed within substations, establishing a network where all devices are interconnected via Ethernet. Consequently, this allows for the exchange of signals and measurements among the devices linked within a local area network [29]. The unit protection schemes used to protect DC SPSs include directional overcurrent and differential protection [30], [31]. Directional overcurrent-based protection in [30] triggers the relay by estimating the overcurrent and the current direction. However, this scheme requires a high sampling rate and proper communication and is limited due to its malfunction in the ring and zonal networks with the normal bidirectional current. Differential protection in [31] requires high guarantees on reliability and speed of communication as the information at both terminals of the DC line must be measured, and it is necessary to carry out data synchronization strictly for both sides' information [32].

For frequency domain-based protections, using a high-frequency component of the transient signals during fault provides an accurate fault detection regardless of the power swing. This method can also be applied in SPS by implementing various schemes, including active impedance-based-protection Fast Fourier transform (FFT) and wavelet-based method. Ref. [33] apply fault detection method using multiresolution analysis of traveling waves that utilizes a discrete wavelet transform to calculate the high-frequency components of DC fault currents. Active impedance based-protection can estimate the system impedance to achieve fault detection and location [8], [34]. This approach involves the injection a very short current spike, followed by an analysis of the transient voltage and current responses to evaluate the bus impedance. However, implementing this scheme necessitates the use of additional injection units, and the rapid calibration of system impedance might introduce errers. An alternative method involves applying FFT to voltage and current measurements to estimate the system impedance during fault conditions, references [35], [36], and [37] applied this method in addition to a communication system based on IEC 61850 for protecting SBMG. The high-frequency equivalent impedance model for converters based on local measurements is studied and analyzed in [38]. However, the estimated impedance of the line is not studied. The wavelet-based method is suitable for analyzing pulse signals by extracting the fault current signal feature at different frequency bands [39], [40]. But it has difficulty in wavelet selections and requires a significant computational burden. However, these schemes cannot detect or locate the fault under different operating conditions, such as the presence of multi-faults or the dynamic behavior of loads and generation sources. Besides, the synchronization process is not investigated. This paper will explore and solve these problems using a powerful proposed scheme. Table 1 compares different protection schemes for shipboard microgrids based on their communication technology, fault clearing time, the cost, advantages, and limitations.

This paper proposes a novel pilot-based unit protection scheme for DC zonal SPSs based on high-frequency impedance estimation. It implements a communication system based on the IEC 61850 protocol considering the synchronization process for data exchanging between the ends of each line simultaneously. Besides, a permissive logic signal is applied to ensure security, sensitivity, and protection speed. To verify the applicability of the proposed scheme, the scheme was simulated in MATLAB/Simulink® program. The proposed scheme is suitably set to apply efficient protection against various scenarios, such as faults at normal conditions, different fault locations, solid and non-solid faults, and simultaneous faults.

The performance of the proposed novel protection method is evaluated under the presence of system uncertainties such as the change in generation, load variations, varying system reconfiguration, and the effect of noise on the communication signals. Although the proposed scheme is simple and doesn't require a significant computational burden, it can detect and locate faults under different conditions in the SBMG system. The main contribution of this paper can be outlined as follows;

- Proposing an innovative unit protection scheme for DC zonal SPSs utilizing pilot-based methods and high-frequency impedance estimation.
- Proposing a novel IED that can exchange the measurement signals after combining a time synchronization source.
- Implementing IEC 61850 communication protocol to transfer the voltage and current measurements at different locations considering the time synchronization.
- Evaluating the performance of the proposed protection method in the presence of system uncertainties such as a change in generation, load variations, varying system

TABLE 1. Comparison of different protection schemes for shipboard microgrid.

Ref	Protection Scheme	Communication Technology	Fault Clearing Time	Cost	Limitations	Advantages
[25]	Overcurrent protection	-	65 ms	Low	Malfunctions during propulsion motor reconfigurations	Simple
[31]	Differential protection	-	27 ms	High	Malfunction occurring during the system complexity.	Accurate and effective.
[41]	Adaptive overcurrent protection	-	36 ms	Low	Malfunction occurring during the system complexity and uncertainty.	Accurate and selective.
[8], [34], [42]	Active impedance estimation	-	200 ms	High	Long fault clearance time. Challenges in determining the frequency for impedance estimation.	Accurate and effective.
[43]	Wavelet transform technique	-	-	High	Complex computations	High Accuracy
[44]	Hybrid discrete wavelet–CNN method	-	-	High	High cost	Reduce the training time compared to other methods with giving the same accuracy.
[45]	Neural Network	-	-	High	Complex	High accuracy in detecting the faults
[46]	Artificial Neural Network	-	-	High	Extended training and computation durations.	Not affected by electrical parameter variations.
[35], [36]	Distance method	IEC 61850	27 - 30 ms	High	Malfunction occurring during the system complexity and uncertainty.	Simple.
Proposed work	High-frequency impedance estimation	IEC 61850	0.125 ms	High	High cost.	Simple Accurate and effective. Not affected by electrical parameter variations. Not affected by the system complexity and uncertainty.

reconfiguration, and the effect of noise on the communication signals.

The paper's structure is as follows: Section II provides an overview of the DC zonal shipboard microgrid. Section III outlines the proposed communication scheme based on IEC 61850. In Section IV, the novel protection scheme is detailed. Section VI presents the simulation verification and corresponding results. Finally, the paper concludes in Section VII.

II. DC ZONAL SBMG SYSTEM ARCHITECTURE

Zonal configuration is a networked distribution system that divides the shipboard loads into n zones. This means that two buses from the port or starboard side feed each zone independently. Zonal distribution can be configured according to IEEE Std. 1709-2010. The US navy standard has adopted this configuration [47]. The zonal distribution system is usually set up on both the port and starboard sides of the ship, with each bus linked at both the stern and bow [48] as shown in Fig. 5. The component of shipboard microgrid architecture is shown in Table 2, where MTG represents the main turbine generator, ATG represents the auxiliary turbine generator, and ESS represents energy storage system. The port and starboard buses are connected to each load. When a fault occurs on one side of the bus, the power sources of vital loads within the zones will automatically switch to the healthy opposite bus. Zonal configuration is beneficial for marine loads. With both port and starboard power, the survivability of the loads is enhanced. When the primary power source is lost, devices switch automatically to the backup power source [49]. This is done to preserve the high-priority, life-sustaining loads such as emergency lighting and fire alarms. The longitudinal bus architecture enables fault isolation when a fault occurs. Coordinated protection systems through a communication network minimize the affected areas during faults. Besides, the ship's line loads are reduced if it is split between the bow and stern. The protection system of such configuration should be more reliable, fast, and provide more survivability.

III. IEC 61850-BASED COMMUNICATION PROTOCOL

The process values of voltage and current from local and remote IEDs at the line terminals are required to implement the proposed scheme. Thus, the process value information has to be transferred from the transmitter of the IED at the remote end to the receiver of the IED at the local end in the form of sampled values (SVs). SV messages require a wide area network (WAN) to be transported between distances over the ship's length. However, these SV messages have only

TABLE 2. Component of shipboard microgrid.

Component	Description
Power Sources	- Main turbine generator (MTG), - Auxiliary turbine generator (ATG). - Renewable Energy Sources (e.g., Solar Panels, Wind Turbines).
Energy Storage System (ESS)	-Battery Banks for Energy Storage
Power Electronics	- Power Inverters for AC to DC Conversion - Converters for Managing Variable Renewable Energy Sources
Communication System	-Communication Network for Interconnecting Components and Data Exchange
Load Centers	-Propulsion - Onboard Loads at each zone.
Protection Systems	- DC circuit breakers for fault isolation -IED for fault detection

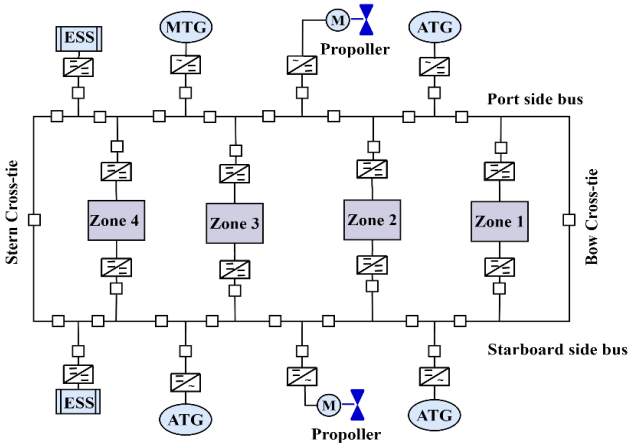

FIGURE 5. DC zonal shipboard microgrid architecture.

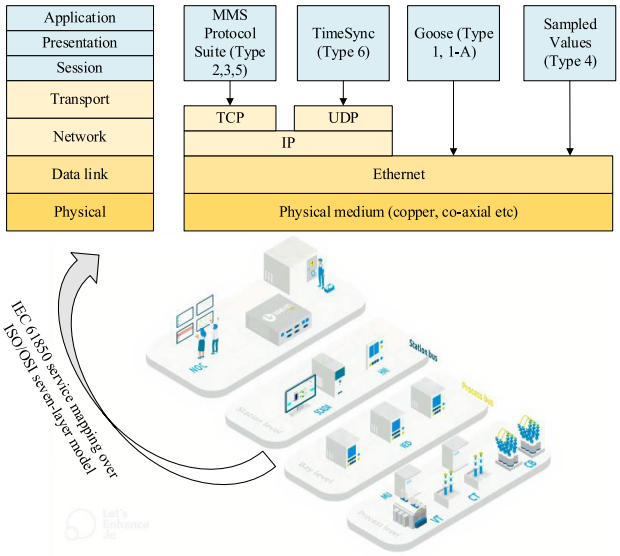

FIGURE 6. IEC 61850 standard levels and its service mapping over ISO/OSI seven-layer model.

a data link layer and do not contain transport and network layers. Thus, to transmit these SV messages over a WAN, IEC 61850 communication protocol is recommended in this paper. IEC 61850 can be mapped onto specific protocols, such as Ethernet, to transfer SV and GOOSE (Generic Object-Oriented Substation Event) messages. GOOSE messages represent burst-type, event-driven communication between geographically dispersed IEDs. In the event of a fault, protective devices generate a burst of GOOSE messages, deviating from their usual periodic heartbeat transmission. This burst mode, illustrated in Ref. [50], exhibits a sequential increase in the retransmission interval until it reverts to the standard periodic pattern after a specified duration. Each message within the burst sequence carries a retransmission timer, indicating the maximum wait time for the subsequent message. If no message is received within this timeframe, the receiver assumes a loss of connection. The setting of the retransmission timer can vary among GOOSE clients. Tailored for SBMG communication, GOOSE messages prioritize rapid, reliable data transfer, critical for prompt fault detection and response. To mitigate damage, trip and block signals must reach their destinations within milliseconds. The proposed IED can model in this paper in which SV messages with Transmission Control Protocol/Internet Protocol (TCP/IP) stack are mapped above the Ethernet layer of the Open Systems Interconnection (OSI) model in the IEC 61850 standard. Fig. 6 shows the mapping of various messages of the IEC 61850 provided over the OSI model. Type 1A and Type 1 messages such as Trip, Start, Close, Stop, etc. are time-sensitive GOOSE messages that directly mapped onto the Ethernet layer in order to reduce the stack. Type-4 messages or raw data are continuous streams of synchronized data from digital instruments transmitted through Ethernet. They are transmitted directly to the Ethernet as a broadcast/multicast address. Type 2, 3, and 5 messages are related to American Customer Satisfaction Indexes (ACSI) applications such as auto-control functions and file transfer messages. They are time-tagged messages and require message-oriented services.

The Multimedia Messaging Service (MMS) protocol with TCP/IP stack is used for these types of messages above the Ethernet layer [50]. SVs and Goose messages are only used in the proposed IED. Goose messages needed to be transported in a WAN and must be routable as it does not have an IP/network layer to be tunnelled. The routers situated at each end of the WAN link create a virtual tunnel, facilitating the transportation of data packets. In this process, the routers encapsulate and decapsulate the data packets, specifically the GOOSE packet, using TCP/IP protocols. The proposed system is considered to be IEC 61850 automated. They have a substation communication network (SCN) composed of similar IEDs. The proposed SPS is made up of three levels: the station, the bay, and the process, as shown in Fig. 6. The station level contains the SPS operating system, engineering stations, and human-machine interfaces (HMIs), which

TABLE 3. Comparison of different communication protocols for shipboard microgrid [51], [52], [53].

Feature	IEC 61850	Modbus	DNP3	Ethernet/IP
Interoperability	High	Moderate	Moderate	Moderate
Standardization	Well-defined, widely adopted	Open standard	Widely used in SCADA	Industrial standard
Data Exchange	Standardized data models and semantics	Simple register-based	Structured data objects	Common Object Model
Network Performance	High efficiency with GOOSE	Moderate	Variable	Fast and deterministic
Fault Tolerance	Built-in redundancy options	Limited	Redundancy features	Redundancy options
Scalability	Easily scalable due to standardized architecture	Limited by design	Scalable architecture	Scalable architecture
Configuration and Maintenance	Easier configuration and maintenance with standardized tools	Manual configuration	Configuration tools	Configuratio n tools
Cybersecurity	Includes security features; integrated security protocols	Basic security	Security features	Security features
Real-time Capabilities	Supports real-time communication	Limited real-time	Real-time capabilities	Real-time capabilities

are used for monitoring and controlling equipment such as transformers and circuit breakers. This level is not included in the proposed scheme but is necessary for the system's operator. One meaningful way to maintain a safe grid is using information from the field, achieved via a proposed protocol that provides voltage and current samples in the MU-IED at the process level. Then, IED sends signals to the breaker for any faults arising in SPSs at the bay level. For SPSs, the utilization of the IEC 61850 standard in our proposed method is aimed at enhancing interoperability, communication efficiency, and standardized data exchange within the power system. IEC 61850 is widely recognized and adopted in the power industry for its capabilities in ensuring seamless communication among IEDs. Table 3 shows a comparison to show the advantages of implementing IEC 61850 against other communication protocols in SPSs.

IV. PROPOSED PROTECTION SCHEME

A unique pilot-based unit protection scheme is employed for DC zonal SPSs in the proposed IED, utilizing high-frequency impedance estimation. To achieve this, FFT is utilized to extract the high-frequency components of voltage and current measurements, which are then used to estimate and compare the system impedance. Moreover, IEC 61850 communication protocol is applied to exchange the measurements and permissive signals between the line terminals. A time synchronization source is also combined to take the measurements at the same instant before exchanging these measurements among IEDs. The time synchronization process is performed using Global Policy and Strategy (GPS) and IEEE 1588, as discussed in [31] and [32]. The steps performed by the proposed IED are explained in detail below.

A. MEASUREMENTS PROCESSING

The voltage and current at each IED are measured and recorded. To smooth the data curve before applying FFT, a Blackman window is used to remove the edge influence of the measured data, which appears after the transformation of the measured data to the frequency domain [8]. It is a function in which finite non-zero values are returned inside a chosen interval, and zero value is returned outside that interval [56]. In the analysis, several factors are considered in choosing the Blackman window over other alternatives like Bartlett, Blackman-Harris, and Flat Top. Each window function has unique characteristics that make it suitable for specific applications. The Blackman window, in particular, offers a balanced combination of low side lobes and narrow main lobes, which is beneficial for our frequency analysis goals. To provide further clarity, a comparison table outlining the key properties of the Blackman window alongside Bartlett, Blackman-Harris, and Flat Top is shown in Table 4. The Blackman window described in [56] can be represented as follows;

$$w(n) = 0.42 - 0.5\cos\left(\frac{2\pi n}{N-1}\right) + 0.08\cos\left(\frac{4\pi n}{N-1}\right), \quad for -\frac{N-1}{2} \le n \le \frac{N-1}{2} \tag{1}$$

where $w(n)$ represents the signal that may be voltage or current, n represents the time index, N represents the length of the Blackman window. After that, the voltage and current measured data are padded to provide a better frequency resolution and increase the data length to improve the impedance estimation method. FFT is applied to the padded voltage and current data to transform it into the frequency domain as follows;

$$F(w(n)) = \sum_{n=0}^{j-1} w(n)\, e^{-\left(i\frac{2\pi nk\Delta t}{j}\right)} \tag{2}$$

where 'k' signifies the frequency index, 'Δt' stands for the sample period, and 'j' indicates the number of samples. Following the high-frequency recording of these measurements, the initiation of the detection process is explained below.

B. HIGH-FREQUENCY IMPEDANCE ESTIMATION SCHEME

Whenever a fault occurs on SPSs, the voltage at the fault point will instantly drop to a lower level, consequently increasing the current. Depending on this concept, an impedance estimation scheme is developed [8], [34]. This scheme estimates the impedance between the IED and faulty points to accurately locate the fault.

To analyze faults in the zonal configuration system shown in Fig. 5, a partial equivalent circuit is shown in Fig. 7. The pole-pole fault can be seen no matter which point the

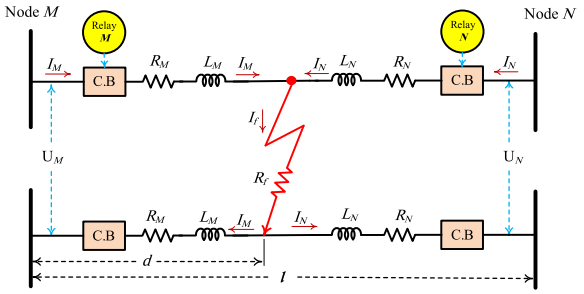

FIGURE 7. High-frequency equivalent circuit of the faulted network.

short-circuit occurs. The resistances R_M, R_N represent the equivalent resistance of the line from the relay point to the fault location, the inductances L_M, L_N represent the equivalent inductance of the line from the relay point to the fault location, and R_f represents the fault resistance.

Before the fault, it is possible to calculate the overall equivalent resistance R_l and inductance L_l of the entire line as follows;

$$R_l = 2R_M + 2R_N \tag{3}$$
$$L_l = 2L_M + 2L_N \tag{4}$$

The value of the line impedance Z_l can be calculated as;

$$Z_l = R_l + j\omega L_l \tag{5}$$

After the fault, the value of the impedance between node M and the fault point (Z) can be expressed as follows;

$$Z = 2R_M + j2\omega L_m \tag{6}$$

A high-frequency impedance estimation scheme can be expressed by applying Kirchhoff's voltage law (KVL) to the equivalent circuit shown in Fig. 7 as follows,

$$U_M = 2R_M I_M + j2\omega L_M I_M + I_F R_f \tag{7}$$
$$U_N = 2R_N I_N + j2\omega L_N I_N + I_F R_f \tag{8}$$

where $U_M \& U_N$ represents the high-frequency component of voltage at node M and node N, respectively, and $I_M \& I_N$ represents the high-frequency voltage component at node M and node N, respectively.

By sharing the voltage of each node and the line current in each segment between IEDs, each IED has its local and remote measurements of the voltage and current. Fault resistance can be eliminated by subtracting the voltage of the two nodes. This allows the voltage difference to be calculated as follows;

$$U_M - U_N = 2R_M I_M - 2R_N I_N + j2\omega L_M I_M - j2\omega L_N I_N \tag{9}$$

The original relation in (9) can be simplified using (3)-(4). The simplified equation is formulated as follows;

$$U_M - U_N = 2R_M I_M - (R_l - 2R_M)\, I_N + j2\omega L_M I_M - j\omega (L_l - 2L_M)\, I_N \tag{10}$$

$$U_M - U_N = 2R_M I_M - R_l I_N + 2R_M I_N + j2\omega L_M I_M - j\omega L_l I_N + j2\omega L_M I_N \tag{11}$$
$$U_M - U_N = 2R_M I_M + 2R_M I_N + j2\omega L_M I_M + j\omega 2L_M I_N - R_l I_N - j\omega L_l I_N \tag{12}$$
$$\Delta U_{MN} = (I_M + I_N)\,(2R_M + j2\omega L_m) - I_N\,(R_l + j\omega L_l) \tag{13}$$

Equation (13) can be simplified by using (5)-(6) as follow;

$$\Delta U_{MN} = Z\,(I_M + I_N) - Z_l I_N \tag{14}$$

Hence, the high-frequency impedance of the network Z can be expressed after applying FFT to both voltage and current signals as follows,

$$Z = \frac{\Delta U_{MN} + Z_l I_N}{I_M + I_N} \tag{15}$$

The formula for calculating fault distance can be derived from Equation (16) as follows:

$$d = \frac{\Delta U_{MN} + Z_l I_N}{(I_M + I_N)(R_U + j\omega L_U)} \tag{16}$$

where d stands for the fault distance, R_U and L_U stand for the unit resistance and unit inductance for the line respectively. The data $\Delta U_{MN}, I_N, and\ I_M$ are measured and transferred to a processor unit.

However, the same principles can be applied to pole-to-ground faults. After estimating the line impedance, it is compared with the pre-calibrated value to detect and locate the fault. The voltage and current signals should be synchronized to enable all IEDs to obtain the data simultaneously and reduce communication errors in the proposed scheme. A modern GPS module is applied, as shown in Fig. 8 [57].

TABLE 4. Comparison between different window functions [58], [59].

Window Function	Side Lobes	Main Lobe Width	Spectral Leakage	Application Suitability
Blackman	Low	Narrow	Very Low	Frequency analysis
Bartlett	Moderate	Moderate	Moderate	Smoothing
Blackman-Harris	Low	Narrow	Low	General purpose
Flat Top	Very Low	Wide	Very Low	Precision amplitude

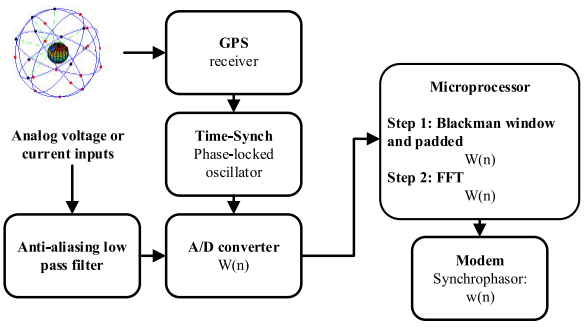

FIGURE 8. Employed synchrophasor measurement equipment internal structure.

Fault can be detected by estimating the high-frequency impedance of the line, which is only related to the line, not the whole system. The proposed method only estimates the line impedance, which is constant under different operation modes. So, the change in loads, changes in generation, change in system configuration, change in fault resistance, and presence of multi-faults don't affect the method for fault detection and localization. After the proposed IED estimates the high-frequency impedance of the line, it checks if it is under the pre-calibrated value. If this condition is achieved, a detecting signal is sent from the IED at the node M shown in Fig. 7 to the IED at the node N. At the same time, a detecting signal is received from the IED at the node N. This communication process is applied before sending the tripping action to C.B related to each IED. The two C.Bs at node M and node N will trip at the same time.

C. PILOT IMPEDANCE ESTIMATION SCHEME

A pilot scheme is utilized when each IED on both ends of the line sends a detecting signal that may be '1' or '0' for detecting or not detecting a fault. In the proposed system, this signal will be sent and received to and from the two IEDs, i.e., each IED will have two signals, the first detecting one and receiving one. Depending on the logical expression below, the tripping signal will be taken accurately before sending it to the related C.B. If both the detecting and received signals are equal to '1', the tripping signal will be '1'. If not, the tripping signal will be '0' as expressed by (17).

$$S = \begin{cases} 1, & S_M \cap S_N = 1 \\ 0, & S_M \cap S_N = 0 \end{cases} \tag{17}$$

where S_M and S_N denote the communication signals sent between the two IEDs at the ends of the DC line, and S denotes the tripping signal sent to the related C.B.

The signals between IED1 and IED2 are sent and received using IEC 61850 communication protocol. as shown in Fig. 9. The communication signals are exchanged between the two IEDs before sending the tripping signals to the corresponding CB to ensure the correct decision for each relay. This pilot scheme enables fault isolation by the two C.Bs at the same time.

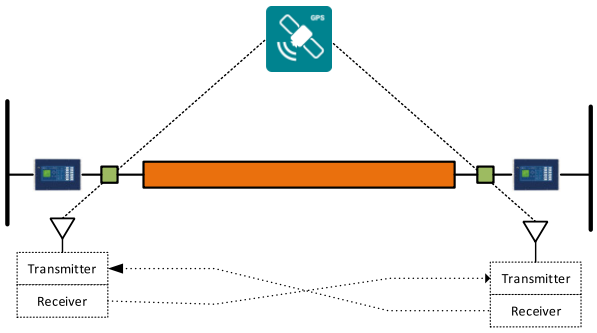

FIGURE 9. Communication mechanism between local and remote ends.

The proposed pilot protection scheme relies on a high-frequency impedance estimation that utilizes the measurements of the proposed synchrophasor. The high-frequency components of these measurements are to be detected by applying FFT. These components are then sent to the remote bus via a high-speed communication channel-based IEC 61850 communication protocol. In this case, local and remote data are used in (15) for both ends of each line to estimate the high-frequency impedance of the line. If both IED1 and IED2, shown in Fig. 9, detect a fault condition, a tripping command is sent to both related C.Bs. However, different factors, such as a detection process, communication delay between IEDs, and circuit breaker operation time, affect the speed of a fault-clearing process. The total clearing time (t_{clear}) can be calculated as follows [60]:

$$t_{clear} = t_{detection} + t_{comm} + t_{CB} \tag{18}$$

where $t_{detection}$ is associated with the detection process in which data gathering windows and measurements are carried out before detecting and locating the fault, t_{comm} represents the communication delay time which depends on the type of communication channel, and t_{CB} represents the CB operating time to isolate the faulty line. The system's sampling frequency is 2000 kHz, resulting in a sampling time of 5 μs. The communication channel bandwidth is 10 Gbps as detailed in [50], providing a communication time of 0.01405 ms. Furthermore, the switching frequency of converters and DC breakers is 10 kHz, resulting in a switching time of 0.1 ms. Considering these values, the total clearing time is over 0.11905 ms.

After synchronizing all IEDs in the system using GPS, a flowchart representing the steps that occurred in the proposed IED is shown in Fig. 10. The steps can be summarized as follow;

- Each IED sensor measures both line voltage and current.
- A Blackman window is applied for the measurements to reduce spectral leakage due to signal truncation.
- Afterward, FFT is employed to process these measurements, extracting voltage and current values at a high frequency of 1000 Hz, in accordance with [23]. These values are subsequently transmitted between the two IEDs responsible for protecting the same line, utilizing the IEC 61850 communication protocol.
- Each IED calculates the line impedance based on Equation (15). Consequently, if the calculated impedance falls below the predetermined threshold for the line, both IEDs on the same line detect a fault.
- The estimated impedances of the two IEDs are sent to each other. If the two IEDs detect a fault, the fault is detected on the line.
- Finally, tripping signals are transmitted to the related CBs to isolate the fault.

V. SIMULATION VERIFICATION

The proposed adaptive protection method has been applied and evaluated using Aquatanker vessel SBMG parameters

within MATLAB/Simulink® as illustrated in Fig. 11. The proposed system comprises of two DC buses, specifically the starboard and portside bus. It is fed by four sources that are two identical batteries, PV and wind turbine. The system is organized into two zones with two loads. The network parameters are listed in Table 5 [61]. Each line in the proposed system is protected by two IEDs, one at the beginning and the other at the end of the line. The communication protocol between all IEDs is shown in Fig. 11, in which all IEDs are communicated with each other through IEC 61850 with GPS to synchronize the data. Different scenarios are applied, and the results are analyzed as follows:

A. Scenario#1 Pole-Pole fault during normal operation.
B. Scenario#2 Faults at different locations of a line.
C. Scenario#3 Different fault resistances.
D. Scenario#4 Simultaneous faults.
E. Scenario#5 Performance evaluation of the proposed scheme in the presence of system uncertainties.

1. Case#1 Change in generations
2. Case#2 Load variations
3. Case#3 Effect of varying system reconfiguration.
4. Case#4: Effect of communication errors on estimation accuracy.

All of these scenarios are discussed below. Also, the clearing time of the proposed method is discussed. The model emplys a sampling frequency of 200 kHz, corresponding to a sampling time of 5μs. Besides, the communication channel boasts a bandwidth of 10 Gbps, equivalent to 7116.778 kHz, allowing for a communication time of 0.1405μs [62]. The switching frequency for all DC circuit breakers and all connected converters is 10 kHz, providing a 100 μs switching time [63].

A. SCENARIO#1: POLE-POLE FAULT DURING NORMAL OPERATION

A pole-pole (P-P) fault is applied in this scenario at F1 on the mid-point of the line at the normal operation, as shown in Fig. 11. The fault resistance is 0.0001 Ω. Fig. 12 shows the system voltage during the fault. The voltage of the faulted section becomes zero, and the voltage of loads #1 and #2 is restored to its nominal value after fault isolation. The currents of IED1, IED3, IED5, load#1, and load#2 are shown in Fig. 13. The current of both loads is 40 A and is restored to its steady-state value after clearing the fault. The measured impedance at 1000 Hz is shown in Fig. 14 after implementing the fault for both IED1 and IED2. The high-frequency impedance estimation is 0.075Ω with a clearing time of 0.17 ms.

B. SCENARIO#2: FAULTS AT DIFFERENT LOCATIONS OF A LINE

Changing the location of the faults may affect the performance of the proposed IEDs and the clearing time for each IED. This scenario explores the performance of the proposed method under various fault location conditions. In this case, after detecting and locating the faults for each IED, the first IED sends a signal to the second IED making it send its tripping action simultaneously and not waiting for its delay time. Multiple P-P faults are implemented at different locations on the line between IED3& IED4 (18% – 50% – 82%) at F2, F3, and F4, as shown in Fig. 11. The fault resistance

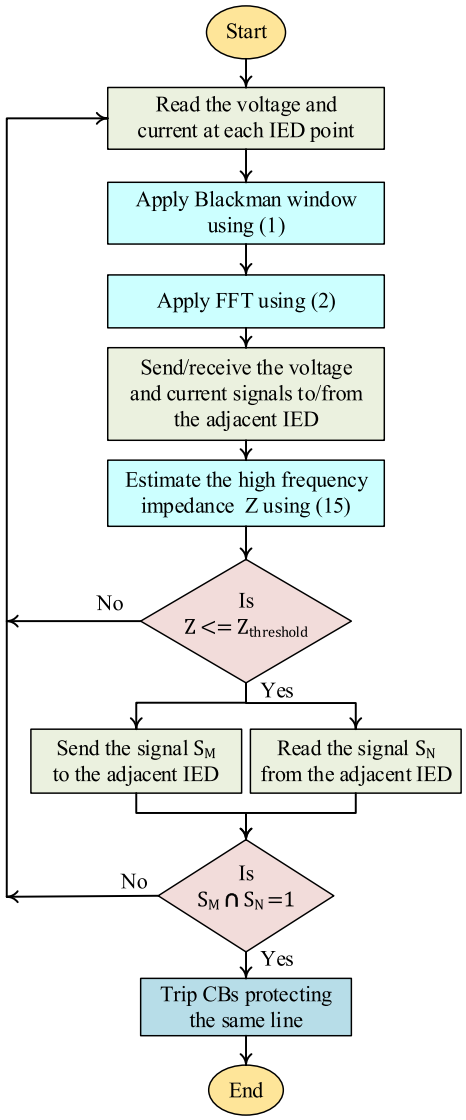

FIGURE 10. Flowchart of the proposed IED.

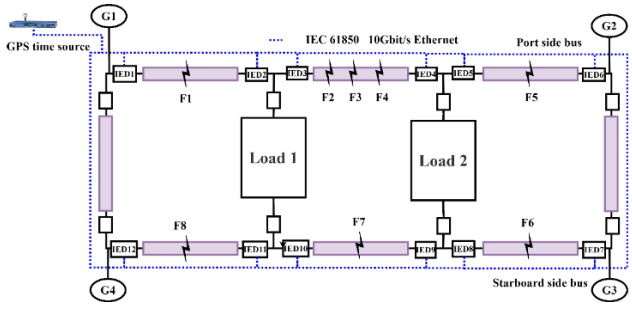

FIGURE 11. Proposed DC Zonal SPS structure.

TABLE 5. Network parameters.

Parameter	Value
Ship length	400 m
Ship width	31 m
Resistance per length	0.32×10-6 Ω/m
Inductance per length	0.17 μH/m
Fault resistance range	0.0001 - 2 Ω
Load zone 1	40 kW
Load zone 2	40 kW
Rated DC voltage	1 kV
Solar cell (G3)	96.3 kW
Wind turbine (G4)	5 kW
Battery (G1, G2)	100 AH

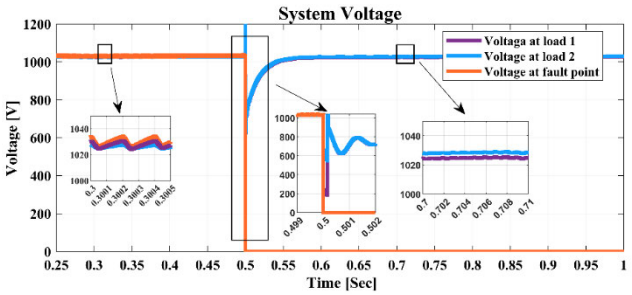

FIGURE 12. DC bus voltage during a P-P fault at F1 (at t=0.5 s).

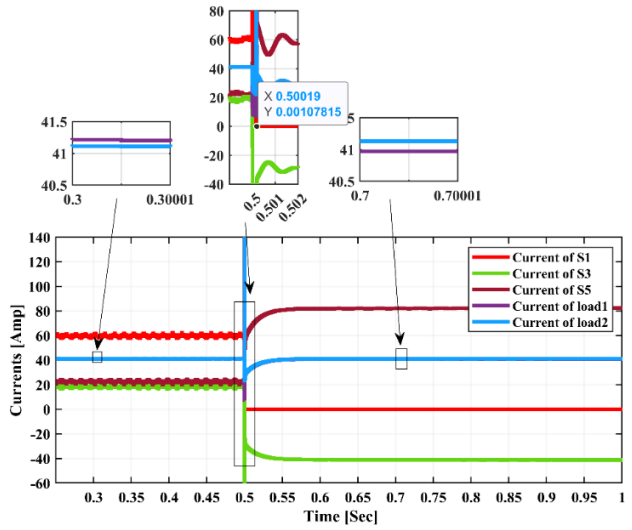

FIGURE 13. Currents during isolation of faulty section by tripping IED1 and IED2.

is taken as 0.0001 Ω. Table 6 shows the clearing time for IED3 & IED4 at different locations with the implementation of permissive communication signals (CTWCS) and without it (CTWOCS). Besides, Table 6 shows the high frequency impedance estimation (HFIE) for IED3 & IED4. The currents of IED3 & IED4 during F2 are shown in Fig. 15, which proves that the IED3 & IED4 isolate the fault simultaneously after 0.125 ms, although they don't have the same clearing time without the communication signals. The measured impedance is shown in Fig. 16 for IED3 & IED4 for all the faults. The proposed method is robust whatever the fault

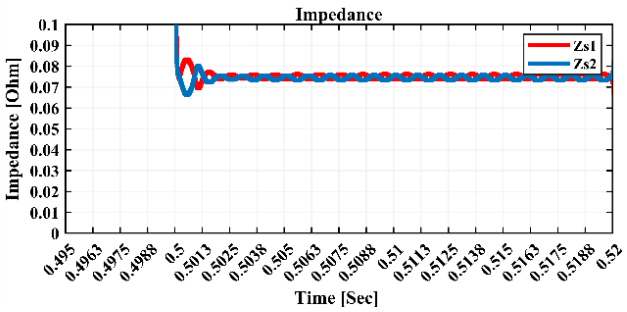

FIGURE 14. Equivalent impedances for IED1 and IED2 with P-P fault at F1 (at t=0.5 s).

TABLE 6. Clearing time and Measured Impedance with and without communication signals.

Fault	IED3			IED4		
Type	CTWOCS	CTWCS	HFIE	CTWOCS	CTWCS	HFIE
F2 (25 m)	0.125 ms	0.125 ms	0.025 Ω	0.135 ms	0.125 ms	0.124 Ω
F2 (67 m)	0.105 ms	0.105 ms	0.075 Ω	0.105 ms	0.105 ms	0.075 Ω
F3 (110 m)	0.135 ms	0.125 ms	0.124 Ω	0.125 ms	0.125 ms	0.025 Ω

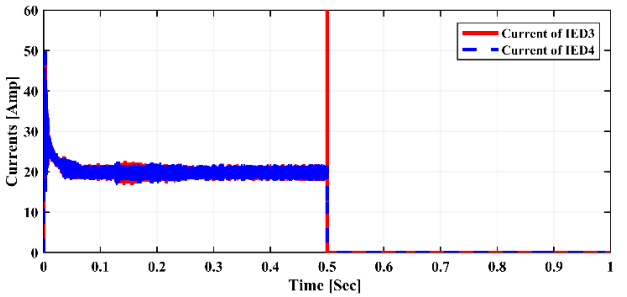

FIGURE 15. Currents of IED3 &IED4 for F2 only.

location is even if it is close to the bus, a pole-pole-ground fault is implemented on the line between IED1&IED2 locating after 1 Ω far from IED1. The fault resistance is taken as 0.0001 Ω. The current of IED1 is shown in Fig. 17 proving that the fault can be detected and isolated after 0.15 ms.

C. SCENARIO#3: DIFFERENT FAULT RESISTANCES

The effectiveness of the proposed protection technique is assessed under various fault resistance scenarios. A P-P fault is implemented at 0.5 sec and located at 75% from IED5 at F5, as illustrated in Fig. 11. The fault is implemeted several times with fault resistances varied between 0.01–2 Ω. The estimated impedances seen by IED5 & IED6 for all faults before sending the tripping signals to the related CBs are shown in Fig. 18. The measured impedance doesn't change with changing the fault resistance, this highlights the superiority of the proposed protection scheme in identifying faults with varying fault resistances.

D. SCENARIO#4: SIMULTANEOUS FAULTS

This case explores the performance of the proposed technique for simultaneous faults. Two P-P faults (F5 and F8) are

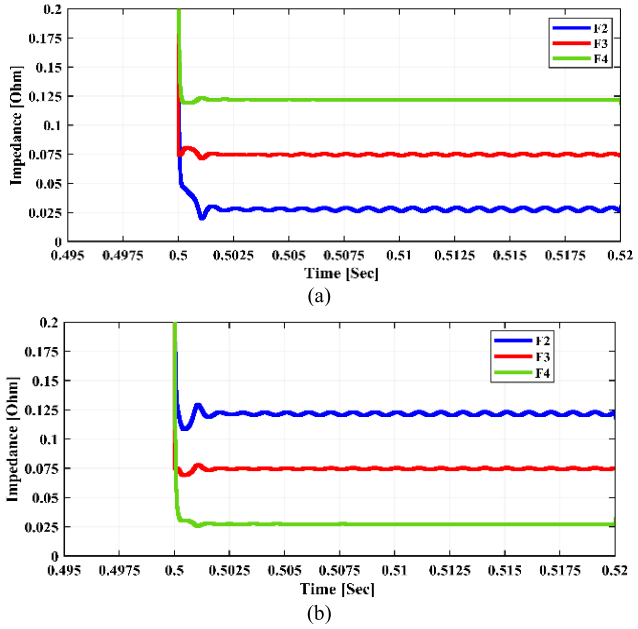

FIGURE 16. Estimated impedance during fault for different fault locations. (a) the impedance at IED3. (b) the impedance at IED4.

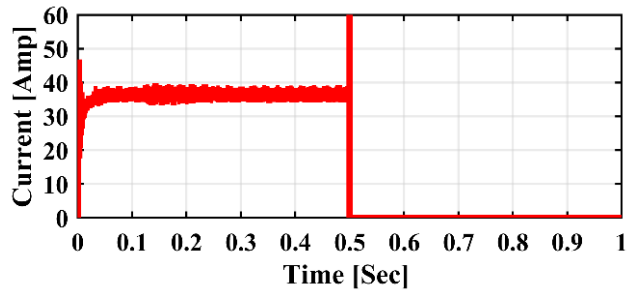

FIGURE 17. Current of IED1 for fault near bus beside IED1.

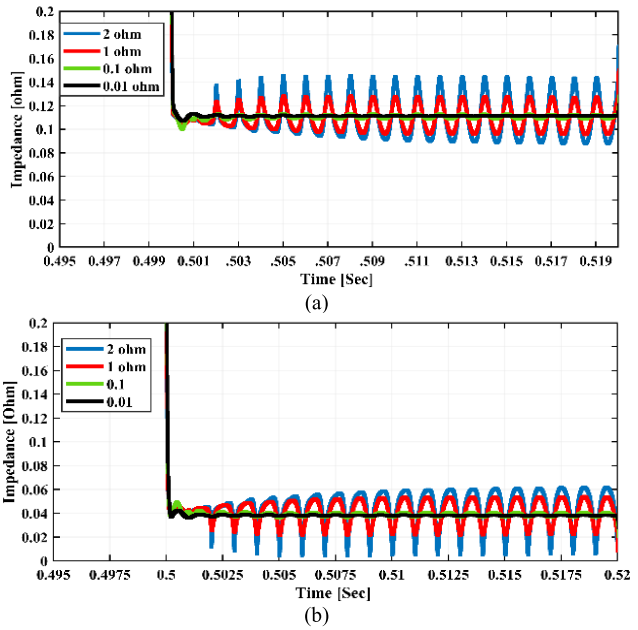

FIGURE 18. Estimated impedance during fault for different fault resistances. (a) the impedance at IED5. (b) the impedance at IED6.

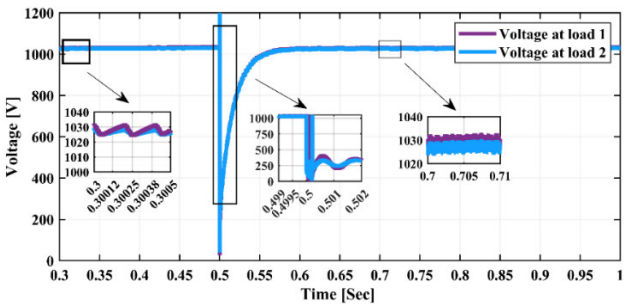

FIGURE 19. System voltage during implementing instantaneous two faults at F5 & F8.

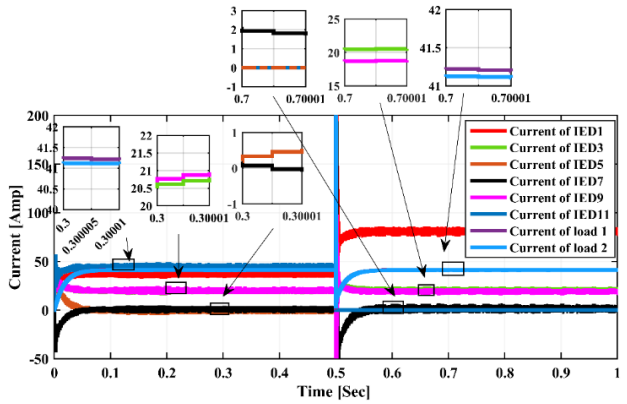

FIGURE 20. Line and Load currents during implementing instantaneous two faults at F5 & F8.

implemented simultaneously for two lines. The first is the line between IED5 and IED6, and the second is the line between IED11 and IED12, as shown in Fig. 11. The two faults, F5 and F8, are applied 15% apart from IED5 and IED12, respectively. The faults are applied at t=0.5 sec with 0.0001 Ω fault resistance. The variation of the system voltage is shown in Fig. 19. The currents of the system's lines and the loads are shown in Fig. 20. In contrast, the estimated impedances of IED5, IED6, IED11, and IED12 are shown in Fig. 21. Table 7 shows the IEDs that sends a tripping signal to their corresponding CBs with their clearing time. The results show the robustness of the proposed methods against simultaneous faults.

E. SCENARIO#5: PERFORMANCE EVALUATION OF THE PROPOSED SCHEME IN THE PRESENCE OF SYSTEM UNCERTAINTIES

Due to the presence of system uncertainties, such as changes in generations, load variations, and varying system reconfiguration, the system performance may be changed. The performance evaluation of the proposed scheme due to the presence of these uncertainties is discussed as follows;

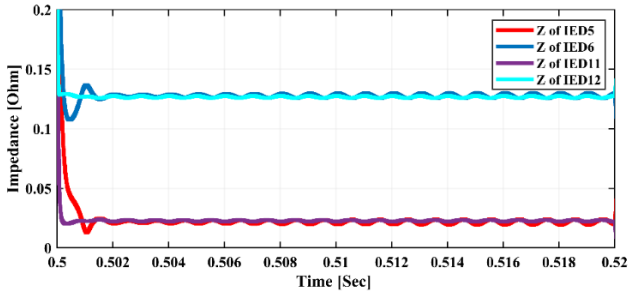

FIGURE 21. Estimated impedance for IED5, IED6, IED11, and IED12 during simultaneous faults at F5 & F8.

TABLE 7. IEDs reconfiguration.

IED	Tripping Signal	Clearing time [ms]
IED1	No	-
IED2	No	-
IED3	No	-
IED4	No	-
IED5	Yes	0.21
IED6	Yes	0.21
IED7	No	-
IED8	No	-
IED9	No	-
IED10	No	-
IED11	Yes	0.125
IED12	Yes	0.125

1) CASE#1: CHANGE IN GENERATIONS

Due to the inconsistency of the PV irradiation throughout the day, there will be considerable variations in the system integrated with a high PV penetration level. This case studies and evaluates the impact of these variations on the proposed scheme. A P-P fault is applied at the mid-point of the line at F7, as shown in Fig. 11, with a fault resistance of 0.0001 Ω. The fault is implemented several times while changing PV irradiation (from 1000 to 800 W/m2). The estimated impedances for both IED9 & IED10 are illustrated in Fig. 22. It can be observed that the estimated impedance is the same regardless of changes in PV irradiation.

2) CASE#2: PERFORMANCE DURING LOAD VARIATIONS

Load variations require a new threshold for conventional protection techniques, as changing the line power flow leads to a change in the measured impedance. Moreover, conventional methods can't differentiate between the current of a sudden load change and a fault current. To prove the effectiveness of the proposed scheme under varying load conditions, assume the load is decreased by 25% for zone#1 and increased by 25% for zone#2. A P-P fault is applied with 0.0001 Ω fault resistance at the line between IED9 & IED10 at 37% apart from IED10. The variation of system voltage during load variations is shown in Fig. 23. The currents of the system lines and loads are shown in Fig. 24. The variation in the loads doesn't affect the estimated impedances measured by IED9 & IED10, as illustrated in Fig. 25.

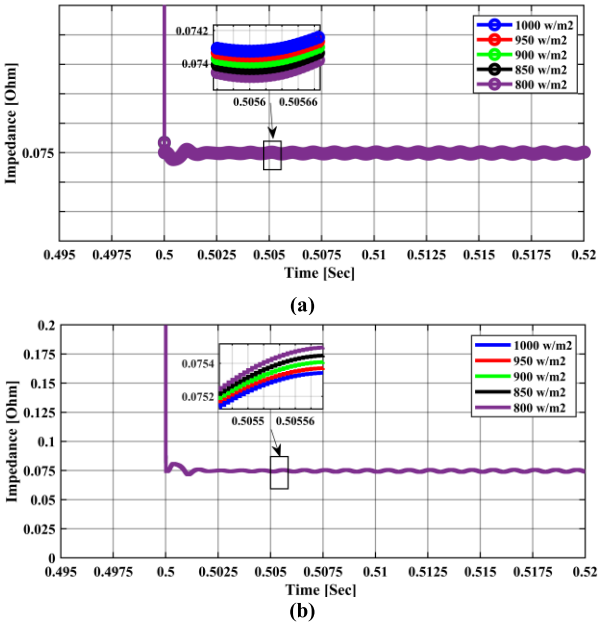

FIGURE 22. Estimated impedance during P-P fault for a change in solar radiation. (a) the impedance at IED9. (b) impedance at IED10.

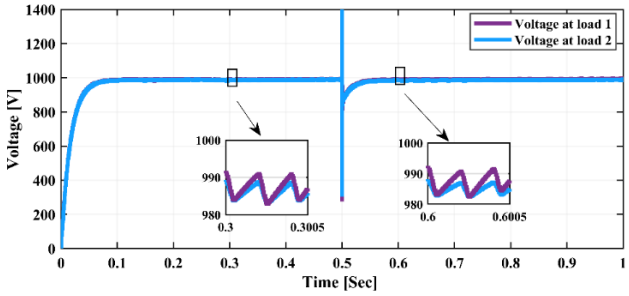

FIGURE 23. DC bus voltage during a pole-to-pole fault at F7 (t=0.5) during Load variations.

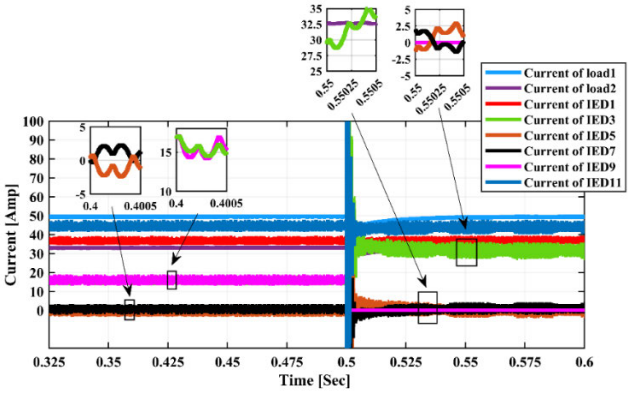

FIGURE 24. System currents during load changing.

3) CASE#3: EFFECT OF VARYING SYSTEM RECONFIGURATION

In this case, a P-P fault is applied at F6 in the mid-point of the line between IED7 & IED8, as shown in Fig. 11. The fault

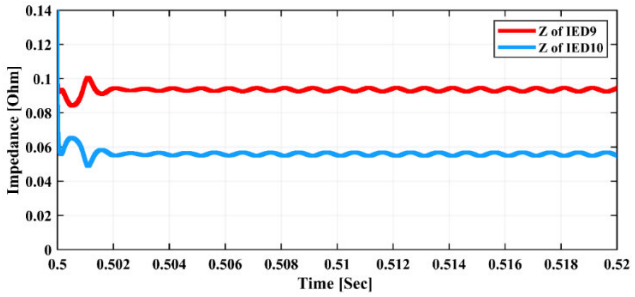

FIGURE 25. Equivalent impedances for IED9 and IED10 for P-P fault at F7 (t=0.5 s).

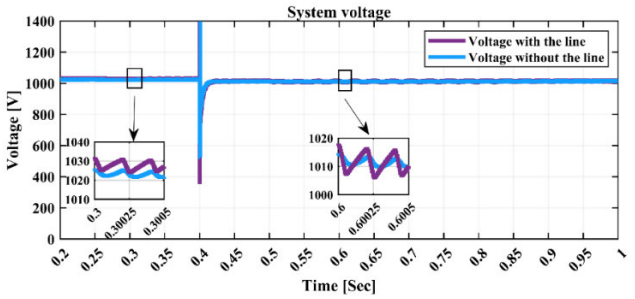

FIGURE 26. System voltage with and without the presence of the line between IED1 & IED2.

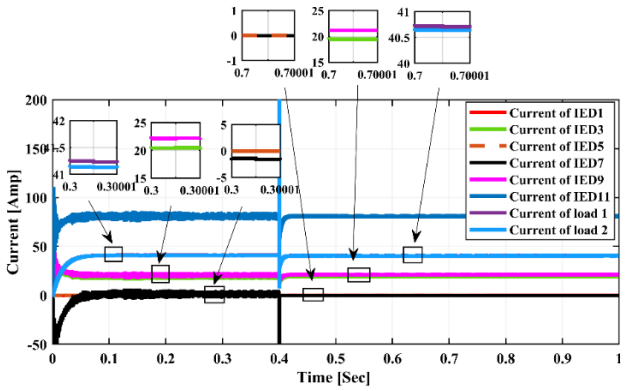

FIGURE 27. System currents in case of the absence of the line between IED1 & IED2.

is implemented twice with and without the presence of the line between IED1 & IED2. The fault resistance is 0.0001 Ω, and it is implemented at 0.4 s. The variation of the system voltage for the two cases is illustrated in Fig. 26. The currents of the system's lines and loads in case of the absence of the line between IED1 & IED2 are illustrated in Fig. 27. The estimated impedances by IED7 & IED8 for the two cases are shown in Fig. 28. It is noticed that the measured impedance is 0.075 Ω for IED7 & IED8 in the two cases. In this case, the measured impedance is not affected by varying the system reconfigurationas. The proposed method depends only on the line impedance and doesn't depend on the whole system impedance.

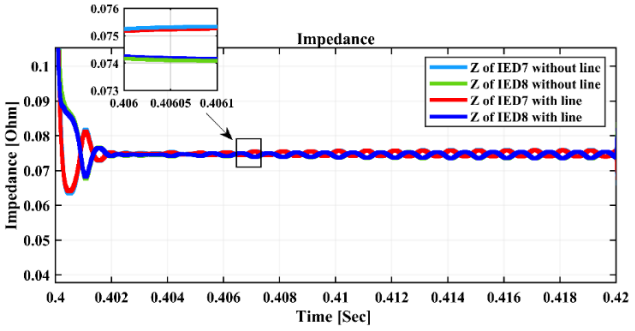

FIGURE 28. Estimated impedances for IED7 and IED8 For P-P fault at F6 (t=0.4 s) with and without the line between IED1 and IED2.

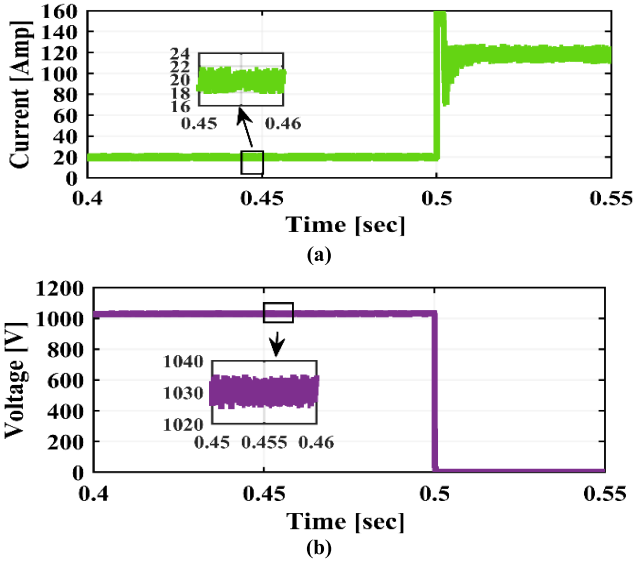

FIGURE 29. Communication signals sent from IED3 to IED4 with 40 dB noise: a) Current signal. b) Voltage signal.

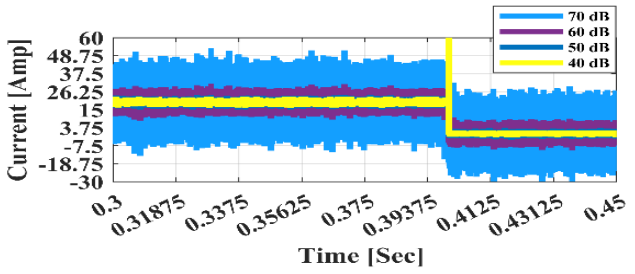

FIGURE 30. Currents of IED3 with different signal to noise ratios.

4) CASE#4: EFFECT OF COMMUNICATION ERRORS ON ESTIMATION ACCURACY

Different noise levels are contaminated in the communication signals to examine how communication errors impact the accuracy of impedance estimation. First, 30 dB band-limited white noise is added to the voltage and current signals sent between IED3 & IED4. The fault is implemented at F2 (18% of the line between IED3 & IED4) shown in Fig. 11. The resulting signals are shown in Fig. 29 before isolating the

TABLE 8. Communication error influence on the estimated impedance.

SNR (dB)	Fault location															
	F1 (50%)		F2 (18%)		F3 (50%)		F4 (82%)		F5 (50%)		F6 (50%)		F7 (50%)		F8 (50%)	
	Estimated impedance error (%)															
	IED1	IED2	IED3	IED4	IED3	IED4	IED3	IED4	IED5	IED6	IED7	IED8	IED9	IED10	IED11	IED12
Without noise	3.28	4.65	6.09	6.2	7.08	7.12	5.13	5.05	6.32	5.89	6.89	7.12	4.33	5.06	3.99	4.39
30	6.8	6.4	9.23	8.98	9.55	9.68	8.85	9.12	8.86	9.66	10.56	9.87	8.87	8.22	9.47	9.97
40	6.87	6.45	10.43	9.28	10.04	11.79	9.07	9.76	8.86	9.69	10.58	9.89	8.89	8.89	9.86	9.97
50	6.87	6.45	10.43	9.28	12.12	11.78	9.82	9.95	8.86	9.69	10.58	9.93	8.89	8.89	9.86	10.56
55	7.25	7.8	10.89	9.89	12.12	11.79	9.88	10.03	10.22	10.12	10.98	9.93	8.89	8.89	10.21	10.89
60	7.89	8.23	11.86	12.3	13.9	13.98	10.22	10.16	10.56	10.77	11.15	9.98	9.56	9.65	10.56	11.36
65	8.58	9.11	11.86	12.3	13.9	13.98	10.22	10.16	11.54	11.12	11.2	10.51	9.56	9.66	11.31	11.36
70	9.88	10.22	11.86	12.3	13.9	13.98	10.22	10.16	12.55	11.14	11.15	11.9	10.2	10.56	12.8	12.3

fault. The simulation results reveal that the high frequency estimated impedance is not significantly affected when applying a wide range of signal-to-noise (SNR) ratios. For a more detailed study, the SNR ratios of 70, 65, 60, 55, 50, 40, and 30 dB are examined for different fault locations at F1, F2, F3, F4, F5, F6, F7, F8, F9, F10, F11, and F12 shown in Fig. 11. The results are tabulated in Table 8. The currents of IED3 after clearing the fault is shown in Fig. 30 after repeating the fault F2 with 70, 60, 50, and 40 dB. The results show a high noise immunity in estimating the high-frequency impedance.

VI. CONCLUSION

This paper introduced an innovative fault detection and localization scheme for DC zonal SPSs based on high-frequency impedance estimation. Leveraging the interoperability of the IEC 61850 protocol, the scheme facilitates seamless data exchange and synchronization between terminals, enabling rapid fault identification. Implemented within an IED and tested in diverse scenarios within a MATLAB/Simulink®environment. Although, the scheme has some limitations such as: the scheme heavily relies on the interoperability of the IEC 61850 protocol for seamless data exchange, and the scheme's performance considerations and potential computational burdens associated with scaling up the system, the proposed technique demonstrates remarkable performance:

- Lightning-fast fault detection and localization: With a clearing time of 0.125ms, the scheme significantly detects the fault at various locations under various conditions.
- Robust impedance estimation: Regardless of operational conditions, the scheme consistently produces accurate and reliable impedance measurements.
- Fault resilience: Independent of fault resistance, generation/load variations, line outages, or communication errors, the scheme effectively detects and locates faults, ensuring system stability.
- Efficiency and simplicity: Minimal computational burden and selective fault identification make the scheme practical and cost-effective."

ACKNOWLEDGMENT

The authors would like to thank Peter Mikulecky, Patrik Urbanik, and Jan Boura for their assistance.

REFERENCES

[1] L. Xu, J. M. Guerrero, A. Lashab, B. Wei, N. Bazmohammadi, J. C. Vasquez, and A. Abusorrah, "A review of DC shipboard microgrids—Part I: Power architectures, energy storage, and power converters," *IEEE Trans. Power Electron.*, vol. 37, no. 5, pp. 5155–5172, May 2022, doi: 10.1109/TPEL.2021.3128417.

[2] A. M. Aboelezz, B. E. Sedhom, M. M. El-Saadawi, A. A. Eladl, and P. Siano, "State-of-the-art review on shipboard microgrids: Architecture, control, management, protection, and future perspectives," *Smart Cities*, vol. 6, no. 3, pp. 1435–1484, May 2023, doi: 10.3390/smartcities6030069.

[3] L. Xu, J. M. Guerrero, A. Lashab, B. Wei, N. Bazmohammadi, J. C. Vasquez, and A. Abusorrah, "A review of DC shipboard microgrids—Part II: Control architectures, stability analysis, and protection schemes," *IEEE Trans. Power Electron.*, vol. 37, no. 4, pp. 4105–4120, Apr. 2022, doi: 10.1109/TPEL.2021.3128409.

[4] A. Latorre, T. B. Soeiro, R. Geertsma, A. Coraddu, and H. Polinder, "Shipboard DC systems—A critical overview: Challenges in primary distribution, power-electronics-based protection, and power scalability," *IEEE Open J. Ind. Electron. Soc.*, vol. 4, pp. 259–286, 2023, doi: 10.1109/OJIES.2023.3294999.

[5] A. M. Aboelezz, A. A. Eladl, M. T. Abo Amasha, M. H. Elderigi, M. A. Mohamed, S. W. Aldoadoa, A. R. Elhamedy, H. M. Alnegeri, T. M. Elshreef, A. A. Eldwany, M. S. Shabka, B. N. Alhasnawi, B. E. Sedhom, and V. Bureš, "Efficient fault detection, localization, and isolation in MT-HVDC systems based on distance protection and LoRaWAN communication," *Energy Rep.*, vol. 10, pp. 4183–4197, Nov. 2023, doi: 10.1016/j.egyr.2023.10.083.

[6] N. Zohrabi, J. Shi, and S. Abdelwahed, "An overview of design specifications and requirements for the MVDC shipboard power system," *Int. J. Electr. Power Energy Syst.*, vol. 104, pp. 680–693, Jan. 2019, doi: 10.1016/j.ijepes.2018.07.050.

[7] M. Babaei, J. Shi, and S. Abdelwahed, "A survey on fault detection, isolation, and reconfiguration methods in electric ship power systems," *IEEE Access*, vol. 6, pp. 9430–9441, 2018, doi: 10.1109/ACCESS.2018.2798505.

[8] K. Jia, E. Christopher, D. Thomas, M. Sumner, and T. Bi, "Advanced DC zonal marine power system protection," *IET Gener., Transmiss. Distrib.*, vol. 8, no. 2, pp. 301–309, Feb. 2014, doi: 10.1049/iet-gtd.2013.0139.

[9] B. J. Brearley and R. R. Prabu, "A review on issues and approaches for microgrid protection," *Renew. Sustain. Energy Rev.*, vol. 67, pp. 988–997, Jan. 2017, doi: 10.1016/j.rser.2016.09.047.

[10] K. Satpathi, A. Ukil, and J. Pou, "Short-circuit fault management in DC electric ship propulsion system: Protection requirements, review of existing technologies and future research trends," *IEEE Trans. Transport. Electrific.*, vol. 4, no. 1, pp. 272–291, Mar. 2018.

[11] A. Dagar, P. Gupta, and V. Niranjan, "Microgrid protection: A comprehensive review," *Renew. Sustain. Energy Rev.*, vol. 149, Oct. 2021, Art. no. 111401, doi: 10.1016/j.rser.2021.111401.

[12] M. Mohammadzamani, I. Sadeghkhani, and M. Moazzami, "Design of a reliable and coordinated protection strategy for zonal shipboard power systems," *IET Electr. Syst. Transp.*, vol. 13, no. 2, pp. 1–25, Jun. 2023, doi: 10.1049/els2.12080.

[13] H. Lan, Y. Bai, S. Wen, D. Yu, Y.-Y. Hong, J. Dai, and P. Cheng, "Modeling and stability analysis of hybrid PV/diesel/ESS in ship power system," *Inventions*, vol. 1, no. 1, p. 5, Mar. 2016.

[14] S. Fang, Y. Xu, H. Wang, C. Shang, and X. Feng, "Robust operation of shipboard microgrids with multiple-battery energy storage system under navigation uncertainties," *IEEE Trans. Veh. Technol.*, vol. 69, no. 10, pp. 10531–10544, Oct. 2020.

[15] Z. Li, Y. Xu, L. Wu, and X. Zheng, "A risk-averse adaptively stochastic optimization method for multi-energy ship operation under diverse uncertainties," *IEEE Trans. Power Syst.*, vol. 36, no. 3, pp. 2149–2161, May 2021, doi: 10.1109/TPWRS.2020.3039538.

[16] A. Y. Hatata, M. A. Essa, and B. E. Sedhom, "Adaptive protection scheme for FREEDM microgrid based on convolutional neural network and gorilla troops optimization technique," *IEEE Access*, vol. 10, pp. 55583–55601, 2022, doi: 10.1109/ACCESS.2022.3177544.

[17] A. N. Sheta, G. M. Abdulsalam, B. E. Sedhom, and A. A. Eladl, "Comparative framework for AC-microgrid protection schemes: Challenges, solutions, real applications, and future trends," *Protection Control Modern Power Syst.*, vol. 8, no. 1, pp. 1–40, Dec. 2023, doi: 10.1186/s41601-023-00296-9.

[18] A. Y. Hatata, M. A. Essa, and B. E. Sedhom, "Implementation and design of FREEDM system differential protection method based on Internet of Things," *Energies*, vol. 15, no. 15, p. 5754, Aug. 2022, doi: 10.3390/en15155754.

[19] B. N. Alhasnawi, B. H. Jasim, and B. E. Sedhom, "Distributed secondary consensus fault tolerant control method for voltage and frequency restoration and power sharing control in multi-agent microgrid," *Int. J. Electr. Power Energy Syst.*, vol. 133, Dec. 2021, Art. no. 107251, doi: 10.1016/j.ijepes.2021.107251.

[20] F. A. Y. Hatata, E. H. Abd-Raboh, and B. E. Sedhom, "A review of anti-islanding protection methods for renewable distributed generation systems," *J. Elect. Eng.*, vol. 16, no. 1, pp. 235–246, 2016.

[21] P. Cairoli, L. Qi, C. Tschida, V. R. R. Ramanan, L. Raciti, and A. Antoniazzi, "High current solid state circuit breaker for DC shipboard power systems," in *Proc. IEEE Electric Ship Technol. Symp. (ESTS)*, Aug. 2019, pp. 468–476, doi: 10.1109/ESTS.2019.8847815.

[22] (2022). *VOSviewer—Visualizing Scientific Landscapes*. Accessed: Aug. 23, 2022. [Online]. Available: https://www.vosviewer.com/

[23] K. Jia, Z. Xuan, T. Feng, C. Wang, T. Bi, and D. W. P. Thomas, "Transient high-frequency impedance comparison-based protection for flexible DC distribution systems," *IEEE Trans. Smart Grid*, vol. 11, no. 1, pp. 323–333, Jan. 2020, doi: 10.1109/TSG.2019.2921387.

[24] M. E. Baran and N. R. Mahajan, "Overcurrent protection on voltage-source-converter-based multiterminal DC distribution systems," *IEEE Trans. Power Del.*, vol. 22, no. 1, pp. 406–412, Jan. 2007, doi: 10.1109/TPWRD.2006.877086.

[25] M. E. Baran, S. Teleke, and S. Bhattacharya, "Overcurrent protection in DC zonal shipboard power systems using solid state protection devices," in *Proc. IEEE Electric Ship Technol. Symp.*, May 2007, pp. 221–224, doi: 10.1109/ESTS.2007.372089.

[26] G. Wu, "Fault detection method for ship equipment based on BP neural network," in *Proc. Int. Conf. Robots Intell. Syst. (ICRIS)*, May 2018, pp. 556–559, doi: 10.1109/ICRIS.2018.00143.

[27] J. A. Momoh and A. S. Ishola-Salawu, "A new arcing fault modeling and detection technique for navy IPS power system," in *Proc. IEEE Power Eng. Soc. Gen. Meeting*, Jun. 2006, p. 7.

[28] H. Erişti, A. Uçar, and Y. Demir, "Wavelet-based feature extraction and selection for classification of power system disturbances using support vector machines," *Electr. Power Syst. Res.*, vol. 80, no. 7, pp. 743–752, Jul. 2010, doi: 10.1016/j.epsr.2009.09.021.

[29] M. García-Gracia, S. Borroy, L. G. de Urtasun, and M. P. Comech, "Novel protection scheme based on IEC61850," *Electr. Power Syst. Res.*, vol. 81, no. 12, pp. 2178–2187, Dec. 2011.

[30] K. Satpathi, N. Thukral, A. Ukil, and M. A. Zagrodnik, "Directional protection scheme for MVDC shipboard power system," in *Proc. 42nd Annu. Conf. IEEE Ind. Electron. Soc.*, Oct. 2016, pp. 3840–3847, doi: 10.1109/IECON.2016.7793893.

[31] J. Tang and P. G. McLaren, "A wide area differential backup protection scheme for shipboard application," *IEEE Trans. Power Del.*, vol. 21, no. 3, pp. 1183–1190, Jul. 2006, doi: 10.1109/TPWRD.2005.860272.

[32] L. L. Qi, A. Antoniazzi, L. Raciti, and D. Leoni, "Design of solid-state circuit breaker-based protection for DC shipboard power systems," *IEEE J. Emerg. Sel. Topics Power Electron.*, vol. 5, no. 1, pp. 260–268, Mar. 2017, doi: 10.1109/JESTPE.2016.2633223.

[33] R. Montoya, B. P. Poudel, A. Bidram, and M. J. Reno, "DC microgrid fault detection using multiresolution analysis of traveling waves," *Int. J. Electr. Power Energy Syst.*, vol. 135, Feb. 2022, Art. no. 107590, doi: 10.1016/j.ijepes.2021.107590.

[34] E. Christopher, M. Sumner, D. W. P. Thomas, X. Wang, and F. de Wildt, "Fault location in a zonal DC marine power system using active impedance estimation," *IEEE Trans. Ind. Appl.*, vol. 49, no. 2, pp. 860–865, Mar. 2013.

[35] A. M. Aboelezz, B. E. Sedhom, and M. M. El-Saadawi, "Pilot distance protection scheme for DC zonal shipboard microgrid," in *Proc. 4th Int. Symp. Adv. Electr. Commun. Technol. (ISAECT)*, Dec. 2021, pp. 01–06, doi: 10.1109/ISAECT53699.2021.9668537.

[36] A. M. Aboelezz, B. E. Sedhom, and M. M. El-Saadawi, "Intelligent distance relay based on IEC 61850 for DC zonal shipboard microgrid protection," in *Proc. 2nd Int. Conf. Power, Control Comput. Technol. (ICPC2T)*, Mar. 2022, pp. 1–5, doi: 10.1109/ICPC2T53885.2022.9776712.

[37] A. M. Aboelezz, M. M. El-Saadawi, A. A. Eladl, and B. E. Sedhom, "IEC 61850 communication-based pilot distance protective IED for fault detection and location in DC zonal shipboard microgrid," *IEEE Trans. Ind. Appl.*, vol. 59, no. 5, pp. 5559–5569, Sep./Oct. 2023.

[38] K. Jia, Q. Zhao, T. Feng, and T. Bi, "Distance protection scheme for DC distribution systems based on the high-frequency characteristics of faults," *IEEE Trans. Power Del.*, vol. 35, no. 1, pp. 234–243, Feb. 2020, doi: 10.1109/TPWRD.2019.2909130.

[39] W. Li, A. Monti, and F. Ponci, "Fault detection and classification in medium voltage DC shipboard power systems with wavelets and artificial neural networks," *IEEE Trans. Instrum. Meas.*, vol. 63, no. 11, pp. 2651–2665, Nov. 2014.

[40] W. Li, M. Luo, A. Monti, and F. Ponci, "Wavelet based method for fault detection in medium voltage DC shipboard power systems," in *Proc. IEEE Int. Instrum. Meas. Technol. Conf.*, May 2012, pp. 2155–2160.

[41] A. A. Memon and K. Kauhaniemi, "Protection of the future harbor area AC microgrids containing renewable energy sources and batteries," *IEEE Access*, vol. 11, pp. 57448–57469, 2023, doi: 10.1109/ACCESS.2023.3283575.

[42] D. Thomas, M. Sumner, D. Coggins, X. Wang, J. Wang, and R. Geertsma, "Fault location for DC marine power systems," in *Proc. IEEE Electr. Ship Technol. Symp.*, Apr. 2009, pp. 456–460, doi: 10.1109/ESTS.2009.4906551.

[43] Z. Ali, Y. Terriche, M. Jahannoush, L. Q. N. Hoang, S. Z. Abbas, and C.-L. Su, "Fault detection and classification in hybrid shipboard microgrids," in *Proc. IEEE PES 14th Asia–Pacific Power Energy Eng. Conf. (APPEEC)*, Nov. 2022, pp. 1–6, doi: 10.1109/APPEEC53445.2022.10072234.

[44] D. Paraskevopoulos, C. Spandonidis, and F. Giannopoulos, "Hybrid wavelet—CNN fault diagnosis method for ships' power systems," *Signals*, vol. 4, no. 1, pp. 150–166, Feb. 2023.

[45] P. A. Lindahl, D. H. Green, G. Bredariol, A. Aboulian, J. S. Donnal, and S. B. Leeb, "Shipboard fault detection through nonintrusive load monitoring: A case study," *IEEE Sensors J.*, vol. 18, no. 21, pp. 8986–8995, Nov. 2018.

[46] N. K. Chanda and Y. Fu, "ANN-based fault classification and location in MVDC shipboard power systems," in *Proc. North Amer. Power Symp.*, Aug. 2011, pp. 1–7, doi: 10.1109/NAPS.2011.6025172.

[47] J. V. Amy, "Considerations in the design of naval electric power systems," in *Proc. IEEE Power Eng. Soc. Summer Meeting*, Jul. 2002, pp. 221–231, doi: 10.1109/PESS.2002.1043244.

[48] G. Sulligoi, D. Bosich, A. Vicenzutti, and Y. Khersonsky, "Design of zonal electrical distribution systems for ships and oil platforms: Control systems and protections," *IEEE Trans. Ind. Appl.*, vol. 56, no. 5, pp. 5656–5669, Sep. 2020.

[49] B. Z. Jin, G. Sulligoi, R. Cuzner, L. Meng, J. C. Vasquez, and J. M. Guerrero, "Next-generation shipboard DC power system: Introduction smart grid and DC microgrid technologies into maritime electrical networks," *IEEE Electrific. Mag.*, vol. 4, no. 2, pp. 45–57, Jun. 2016.

[50] M. A. Aftab, S. Roostaee, S. M. S. Hussain, I. Ali, M. S. Thomas, and S. Mehfuz, "Performance evaluation of IEC 61850 GOOSE-based inter-substation communication for accelerated distance protection scheme," *IET Gener., Transmiss. Distrib.*, vol. 12, no. 18, pp. 4089–4098, Oct. 2018.

[51] I. Alsmadi, Z. Dwekat, R. Cantu, and B. Al-Ahmad, "Vulnerability assessment of industrial systems using shodan," *Cluster Comput.*, vol. 25, no. 3, pp. 1563–1573, Jun. 2022, doi: 10.1007/s10586-021-03330-3.

[52] O. A. T. Rosero, R. J. S. Isaza, G. D. Z. Madrigal, and J. C. Olaya, "Relevant aspects for interoperability in electrical substations under implementation of process bus IEC 61850–9–2 with multi-vendor devices," in *Proc. FISE-IEEE/CIGRE Conf. Living Energy Transition (FISE/CIGRE)*, Dec. 2019, pp. 2–7, doi: 10.1109/FISECIGRE48012.2019.8984957.

[53] J. A. Kay, D. C. Mazur, and R. A. Entzminger, "Basics of communication networks for electrical engineers in the forest products industries," in *Proc. IEEE IAS Pulp, Paper Forest Industries Conf. (PPFIC)*, Jun. 2018, pp. 1–12.

[54] P. A. Crossley, H. Guo, and Z. Ma, "Time synchronization for transmission substations using GPS and IEEE 1588," *CSEE J. Power Energy Syst.*, vol. 2, no. 3, pp. 91–99, Sep. 2016, doi: 10.17775/CSEEJPES.2016.00040.

[55] M. Han, H. Guo, and P. Crossley, "IEEE 1588 time synchronisation performance for IEC 61850 transmission substations," *Int. J. Electr. Power Energy Syst.*, vol. 107, pp. 264–272, May 2019, doi: 10.1016/j.ijepes.2018.11.036.

[56] S. Chakraborty, "Advantages of Blackman window over Hamming window method for designing FIR filter," *Int. J. Comput. Sci. Eng. Technol.*, vol. 4, no. 8, pp. 1181–1189, 2013.

[57] T. G. Bolandi, M. R. Haghifam, and M. Khederzadeh, "Real-time monitoring of zone 3 vulnerable distance relays to prevent maloperation under load encroachment condition," *IET Gener., Transmiss. Distrib.*, vol. 11, no. 8, pp. 1878–1888, Jun. 2017.

[58] B. Taheri, S. A. Hosseini, M. Sedighizadeh, and M. Khatibi, "A moving window numerical distance protection based on flat-top signal windowing," *Arabian J. Sci. Eng.*, vol. 47, no. 11, pp. 14249–14266, Nov. 2022, doi: 10.1007/s13369-022-06709-5.

[59] B. Taheri and M. Sedighizadeh, "A moving window average method for internal fault detection of power transformers," *Cleaner Eng. Technol.*, vol. 4, Oct. 2021, Art. no. 100195, doi: 10.1016/j.clet.2021.100195.

[60] X. Feng, L. Qi, and J. Pan, "A novel fault location method and algorithm for DC distribution protection," *IEEE Trans. Ind. Appl.*, vol. 53, no. 3, pp. 1834–1840, May 2017.

[61] P. Pan, Y. Sun, C. Yuan, X. Yan, and X. Tang, "Research progress on ship power systems integrated with new energy sources: A review," *Renew. Sustain. Energy Rev.*, vol. 144, Jul. 2021, Art. no. 111048, doi: 10.1016/j.rser.2021.111048.

[62] N. H. Ali, B. M. Ali, M. L. Othman, and K. M. Abdel-Latif, "Performance of communication networks for integrity protection systems based on travelling wave with IEC 61850," *Int. J. Electr. Power Energy Syst.*, vol. 95, pp. 664–675, Feb. 2018, doi: 10.1016/j.ijepes.2017.09.024.

[63] A. A. Eladl, M. A. Saeed, B. E. Sedhom, and J. M. Guerrero, "IoT technology-based protection scheme for MT-HVDC transmission grids with restoration algorithm using support vector machine," *IEEE Access*, vol. 9, pp. 86268–86284, 2021.